

EPSC2018

OPS5/TP11 abstracts

Comparison of soluble and insoluble organic matter in analogues of Titan's aerosol

J. MAILLARD^{1,2,*}, N. CARRASCO¹, I. SCHMITZ-AFONSO², T. GAUTIER¹ and C. AFONSO²

(1) LATMOS/IPSL, Université Versailles St Quentin, UPMC Université Paris 06, CNRS, 11 blvd d'Alembert, 78280 Guyancourt, France,

(2) Université de Rouen, Laboratoire COBRA UMR 6014 & FR 3038, IRCOF, 1 Rue Tesnière, 76821 Mont St Aignan Cedex, France, julien.maillard@ens.uvsq.fr

Abstract

The study of Titan's photochemical haze is thus a precious tool to gain knowledge on the primitive atmosphere of Earth. The simulation in the laboratory of analogs of this haze has proved itself to be a useful tool to improve our knowledge of the aerosols formation on Titan. Tholins (analogues of aerosols) produced by PAMPRE experiment were found to be mostly insoluble, with only a third of the bulk sample that can be solubilized in methanol [1]. This partial solubility limited the previous studies by mass spectrometry, which were done only on the soluble fraction. In this work, we compared both soluble and insoluble fraction of tholins in methanol using an ultra-high resolution mass spectrometer equipped with a Laser desorption ionization (LDI) source, to get full insights on these complex samples. Major differences are observed in the molecular composition of the soluble and the insoluble fraction [2].

1. Introduction

It was postulated that soluble and insoluble fractions of Titan's aerosols analogues might be identical at the molecular level and differed on their mass value [3]. Thanks to laser desorption ionization (LDI) source, which allows an ionization of both liquid and solid state, it is possible to compare all fractions.

The goal of this work is to highlight differences between each fractions of analogues of Titan's aerosols.

2. Method

2.1. Sample preparation for analysis

Tholins were produced using the PAMPRE experiment and following the procedure detailed in previous publications [4]. In order to separate soluble and insoluble fractions, 4 mg of tholins were dissolved in 1 mL of methanol in a vial under ambient atmosphere. The vial was vigorously stirred for 3 minutes to dissolve the maximum amount of species. The brown mixture was then filtered using a 0.2 µm polytetrafluoroethylene (PTFE) membrane filter on a filter holder. Of the filtered solution, the soluble fraction, was transferred in a glass vial. Half dilution with a 50/50 water/methanol mixture was performed just before analysis in mass spectrometry. The PTFE membrane was then recovered, placed in a vial and left open under a neutral atmosphere of Nitrogen to evaporate the remaining methanol and avoid contamination. The insoluble fraction, recovered as a black powder from the membrane, was then analyzed by mass spectrometry.

2.2. Mass spectrometry analyses

All analyses were performed on a FTICR Solarix XR from Bruker equipped with a 12 Tesla superconducting magnet and a laser desorption ionization source (laser NdYAg 355 nm).

An extremely complex matter is revealed and graphical analysis is necessary to simplify the visualization of the data. Using modified Van Krevelen diagrams, the global distribution of the molecules is observed in each fraction according to

their Hydrogen/Carbon ratio and Nitrogen/Carbon ratio (Figure 1). From these experiments it appears that the molecular composition is very different between each fraction with the formation of different polymeric structures. Soluble and insoluble fractions while emerging from the same set of molecules at low m/z actually represent two families of compounds that are totally uncorrelated at higher m/z values.

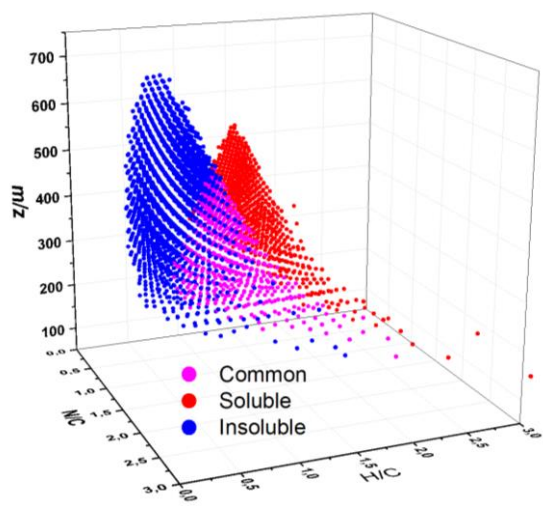


Figure 1: 3D modified Van Krevelen diagrams showing the comparison of (red) soluble species, (blue) insoluble species and (purple) common species in Tholins [2].

3. Summary and Conclusions

This work highlighted, for the first time, major differences between soluble and non-soluble part of analogues of Titan's aerosols. Thanks to the comparison of spectra and global data visualization, we proved that non-soluble fraction is much less hydrogenated than soluble one.

In addition, we bring to light a phenomenon which can occur on the surface of Titan: the fragmentation of aerosols due to their interaction with liquid lakes present on the surface.

Acknowledgements

N.C. thanks the European Research Council for funding via the ERC PrimChem project (grant agreement No. 636829.).

Financial support from the National FT-ICR network (FR 3624 CNRS) for conducting the research is also gratefully acknowledged.

This work was supported at COBRA laboratory by the European Regional Development Fund (ERDF) N°31708, the Région Normandie, and the Labex SynOrg (ANR-11-LABX-0029).

References

- [1] Szopa C. et al., PAMPRE: A dusty plasma experiment for Titan's tholins production and study. *Planetary and Space Science*, 2006. **54**(4), 394-404.
- [2] Maillard J. et al., Comparison of soluble and insoluble organic matter in analogues of Titan's aerosol. *EPSL*, 2018 In press.
- [3] Gautier T. et al., Nitrogen incorporation in Titan's tholins inferred by high resolution orbitrap mass spectrometry and gas chromatography-mass spectrometry. *Earth and Planetary Science Letters*, 2014. **404**, 33-42.
- [4] Gautier, T. et al., Nitrile gas chemistry in Titan's atmosphere. *Icarus*, 2011. **213**, 625-635.

Expanded line-of-sight extinction measurements from the Mars Science Laboratory at Gale Crater, Mars

Christina L. Smith (1), John E. Moores (1), Casey Moore (1), and Scott D. Guzewich (2)

(1) Center for Earth, Space Science and Engineering, York University, Toronto, Canada (chrsmith@yorku.ca)

(2) NASA Goddard Space Flight Center, Greenbelt, Maryland, USA.

Abstract

In this abstract we present updates and expansions to the line-of-sight extinction measurements taken by the Mars Science Laboratory Rover at Gale Crater. We update the single frame line-of-sight dust extinction record through to beyond sol 2000, and extend this work using a combination of two radiative transfer algorithms to expand the dataset beyond north pointing images taken at noon LTST.

1. Introduction

Gale Crater, the landing site of the Mars Science Laboratory Rover, Curiosity, is a 154 km impact crater situated at 4.5° S and 137.4° E on the Martian surface, in the centre of which is Aeolis Mons (colloquially known as Mount Sharp), a 5 km high mountain. The topography of Gale Crater has important implications for atmospheric mixing and aerosol abundance distributions. Before Curiosity arrived on Mars, investigations into the atmospheric circulation in the vicinity of Gale Crater were carried out (e.g. [9, 10]) predicting a suppressed thickness of the planetary boundary layer (the lowest layer of the atmosphere, affected dynamically by the presence of the planet's surface) from 8-10 km outside the crater, to 1-2 km within it. This, in essence, isolates the crater with only minimal atmospheric mixing with the air outside of the crater occurring, making Gale Crater of particular interest for atmospheric dust abundance studies. One of the observable effects of a suppression of the planetary boundary layer is a decrease in the abundance of dust in the lower atmosphere.

In this abstract, we update the noon-time line-of-sight (LOS) dust extinction measurements of [3, 4] through to the present day (sol 2034 at the time of writing). We will then discuss the preliminary work and results obtained by expanding the measurements of the line-of-sight extinction within Gale Crater beyond the time and pointing restrictions using a combination of

radiative transfer models.

2. North-pointing noon LOS

Observations have been consistently obtained with MSL's Navigational Cameras (Navcam) since sol 100, initially using Dust Devil Search Movies (DDSM), created to look for Dust Devils in the northern reaches of Gale Crater. Single frames from these observations were used [3, 4] to determine the line-of-sight extinction between MSL and the crater rim. After sol 1582, when this particular version of the Dust Devil search movies was retired in favour of others, these observations were reduced to a single frame to continue this line-of-sight extinction record. In both cases, DDSM and single-frame, the observation points due north and includes regions of the sky, crater rim, and ground in the vicinity of the rover. As derived in [5], the opacity, τ and thus the LOS extinction ($= \tau/d$ where d is the distance between the rover and the crater rim) can be calculated via:

$$\tau = -\ln \left(\frac{1 - I_S/I_C}{I_G/I_C - I_S/I_G} \right) \quad (1)$$

where I_S , I_C , and I_G are the spectral radiances of the sky, crater rim, and ground respectively, as measured from the Navcam images. This relation is accurate to within 4% during the 12:00 ± 02:00 LTST, as shown by radiative transfer models carried out at Texas A&M University (see [5] for further details).

3. Temporally expanded LOS

These single frame LOS and DDSM observations have been obtained outside of the 10:00-14:00 LTST time period, but retaining the northern pointing. Since sol 1582, they have been obtained in every other morning suite - a weekly set of early morning observations designed to examine the atmospheric conditions before daytime atmospheric heating, and thus dust lifting and cloud dissipation, has occurred. They also, more

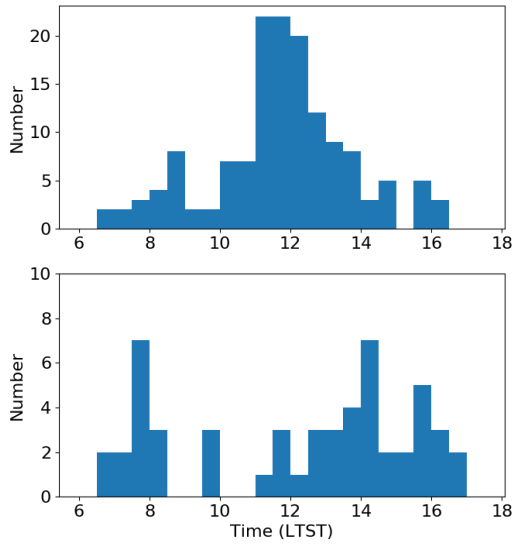


Figure 1: Diurnal distribution of single frame (lower) and DDSMs (upper) for sol 100 to 2034. Note the different y axis scales between the upper and lower panels.

rarely, have been obtained later in the day to constrain the diurnal variation in extinction. Figure 1 shows the LTST distribution of all DDSMs (circles) and single-frame Navcam LOS observations (crosses).

To analyse these observations, we use a combination of radiative transfer algorithms: the plain parallel doubling and adding (D&A, [1]) code used in [6, 8] and Hyperion [7], a 3D radiative transfer code, able to accurately model the topography of Gale Crater. The topography of Gale Crater is taken from the 3D digital elevation model (DEM) constructed from High/Super Resolution Stereo Camera images (HRSC) on-board the Mars Express orbiter [2]. The D&A code is used to determine the sky radiance as a function of time of day and season - for further details see [8].

Ultimately this work will expand to encompass all possible Navcam images that include regions of the sky, crater rim, and ground near the rover to give as complete a view as possible of the dust extinction record in Gale Crater possible. These will subsequently be used to produce a quantitative analysis of the dust deposition rate within Gale Crater as a function of time.

References

- [1] C. A. Griffith et al. Radiative transfer analyses of Titan’s tropical atmosphere. *Icarus* , 218:975–988, Apr. 2012.
- [2] K. Gwinner et al. Topography of Mars from global mapping by HRSC high-resolution digital terrain models and orthoimages: Characteristics and performance. *Earth and Planetary Science Letters*, 294:506–519, June 2010.
- [3] C. A. Moore et al. A full martian year of line-of-sight extinction within Gale Crater, Mars as acquired by the MSL Navcam through sol 900. *Icarus*, 264:102–108, Jan. 2016.
- [4] C. A. Moore et al. Atmospheric Dust Loading Variability in Northern Gale Crater, Mars. In Prep. for *Icarus*, 2018.
- [5] J. E. Moores et al. Observational evidence of a suppressed planetary boundary layer in northern Gale Crater, Mars as seen by the Navcam instrument onboard the Mars Science Laboratory rover. *Icarus*, 249:129–142, Mar. 2015.
- [6] J. E. Moores, C. L. Smith, and A. C. Schuerger. UV production of methane from surface and sedimenting IDPs on Mars in light of REMS data and with insights for TGO. *Planet. Space Sci.* , 147:48–60, Nov. 2017.
- [7] T. P. Robitaille. HYPERION: an open-source parallelized three-dimensional dust continuum radiative transfer code. *A&A* , 536:A79, Dec. 2011.
- [8] C. L. Smith and J. E. Moores. Geometric shielding of surface rocks on Mars. submitted to *Icarus*, 2018.
- [9] D. Tyler, Jr. and J. R. Barnes. Mesoscale Modeling of the Circulation in the Gale Crater Region: An Investigation into the Complex Forcing of Convective Boundary Layer Depths. *International Journal of Mars Science and Exploration*, 8:58–77, 2013.
- [10] A. R. Vasavada et al. Assessment of environments for mars science laboratory entry, descent, and surface operations. *SSR*, 170(1):793–835, 2012.

Evolution of organic aerosols under conditions similar to Titan's ionosphere

A. Chatain (1,2), N. Carrasco (1), O. Guaitella (2), N. Ruscassier (3)

(1) LATMOS, CNRS, Université Versailles St-Quentin, Sorbonne Universités, 78280 Guyancourt, France

(2) LPP, CNRS, Ecole Polytechnique, Sorbonne Universités, Université Paris XI, 91128 Palaiseau, France

(3) LGPM, Ecole Centrale-Supélec, 91190 Gif-sur-Yvette, France

(audrey.chatain@latmos.ipsl.fr)

Abstract

Titan's ionosphere is a dusty plasma where complex organic aerosols are formed. As they have a strong prebiotic interest, we would like to understand how they are formed and how they interact with the surrounding plasma. Here we simulate this interaction dust-plasma in a DC reactor. We place analogues of Titan's aerosols in a N_2 - H_2 discharge and follow their infrared absorption spectrum all along the exposure. The evolution of the surface state of the sample is also observed by scanning electron microscopy. First experiments indicate some modifications in the absorption bands and in the surface structure. Therefore, the organic aerosols seem to be physically and chemically altered by the plasma.

1. Introduction

Atmospheric aerosols play an important role in the climate of planets. Especially, Titan produces such a quantity of particles that its surface becomes invisible from above. The Cassini-Huygens mission discovered that this matter is created high in the atmosphere of the moon, where solar radiations and Saturn's energetic particles can ionize nitrogen and methane of Titan's atmosphere. This leads to complex chemical processes and the formation of organic nanograins in the ionosphere [1].

Laboratory simulations succeed in forming similar organic grains ("tholins") using RF plasma or UV light. Aerosols form in a few minutes and these first chemical steps are relentlessly studied. However, on Titan the particles cross the wide ionosphere during their descent and stay a while in a harsh plasma environment. Especially, the organic grains are likely to evolve physically and / or chemically. [2] recently studied the effect of UV radiations on tholins. Here we look at their evolution under plasma conditions.

2. Experimental setup

2.1 Sample synthesis

Samples are formed in the reactor PAMPRE [3]. A CCP RF discharge is ignited at 30W in a gas mixture of 95% N_2 and 5% CH_4 at 0.9mbar. In a few minutes it leads to the formation of organic grains.

Tholins are then diluted with 99% KBr and pressed in thin pellets.

2.2 Exposure in a plasma reactor

The pellets are exposed during several hours to a N_2 - H_2 plasma. They are put in the middle of a DC glow discharge under a current of 20mA. A flow of 5sccm goes through the tube leading to an adjustable pressure of 1 to 3mbar. Methane is removed from the gas mixture to prevent the formation of new tholins.

2.3 Analysis of the sample evolution

The structure of the sample's surface is examined before and after exposure thanks to an Environment Scanning Electron Microscope (E-SEM) at LGPM (Quanta 200 from FEI).

Besides, the plasma reactor is adapted to fit inside the sample compartment of a FTIR (Bruker V70 with a 0.16cm⁻¹ resolution). This allows direct *in situ* measurement through the pellet under direct plasma exposure. The evolution of tholins are then followed by infrared absorption spectroscopy, in transmission through the pellet.

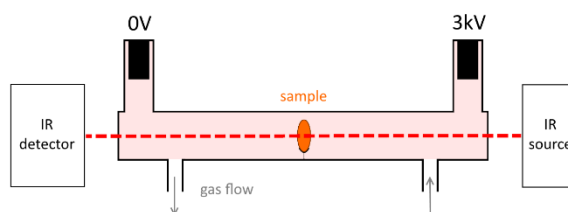


Figure 1: experimental setup

3. Results

3.1 Physical erosion

Pellets are quickly modified when the plasma is ignited. Plasma sputtering makes them whiter, rougher and eroded on the sides.

SEM pictures confirm the preferential erosion of organic material and the global formation of rough structures at the surface

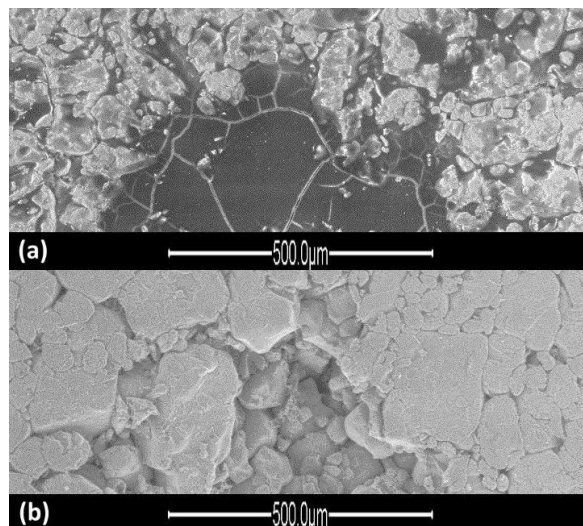


Figure 2: (a) Pellet with 1.5% of tholins in KBr. (b) Same pellet after 4h exposure to plasma at 3torr.

In addition, absolute IR absorbance of eroded pellets attests the loss of absorbing matter and the augmentation of diffusion with roughness.

3.2 Chemical modifications

After normalizing IR absorption bands to remove the effects due to physical erosion, we can notice some distortions in the spectra during plasma exposure.

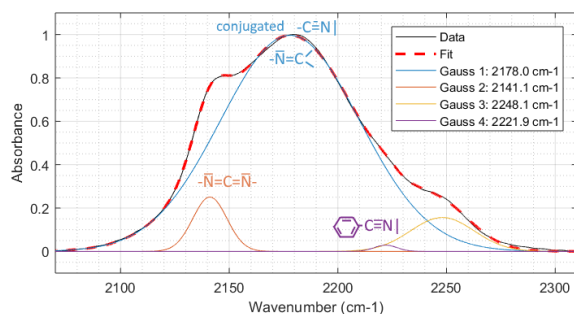


Figure 3: Deconvolution in Gaussians of the nitrile band before exposure

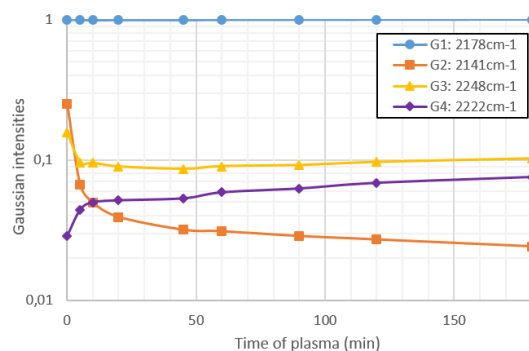


Figure 4: Evolution of Gaussian's amplitudes during exposure

4. Perspectives

Tholins are chemically changed by N_2-H_2 plasma conditions. The next logical step is to modify plasma parameters to understand the role of each species (electrons, ions, radicals...) in the evolutions seen.

Acknowledgements

NC acknowledges the financial support of the European Research Council (ERC Starting Grant PRIMCHEM, Grant agreement no. 636829).

AC is grateful to ENS Paris-Saclay Doctoral Program for its financial support.

References

- [1] Lavvas, P., Yelle, R. V. et al. Aerosol growth in Titan's ionosphere. Proceedings of the National Academy of Sciences, 110(8), 2729-2734, 2013
- [2] Carrasco, N., Tigrine, S. et al. The evolution of Titan's high-altitude aerosols under ultraviolet irradiation. Nature Astronomy, 1, 2018
- [3] Szopa, C., Cernogora, G. et al. PAMPRE: A dusty plasma experiment for Titan's tholins production and study. Planetary and space Science, 54(4), 394-404, 2006

Methane and ethane adsorption and nucleation on tholins

P. Rannou (1), D. Curtis (2), D. Cordier(1)

(1) GSMA, Université de Reims Champagne-Ardenne, FRANCE (2) Department of Chemistry and Biochemistry
 California State University, Fullerton, CA, UNITED-STATES

Abstract

The nucleation properties of methane and ethane on tholins depends upon few specific key parameters which are generally poorly defined ; the wetting parameters m (equal to the cosine of the contact angle made by the embryo on the substrate) and the desorption energy of the condensing species on the substrate, ΔF_{des} . Often, wetting parameter are found in the range [0.9-1.0] to promote cloud formation. The desorption energies are taken from experimental results on substrates approximatively similar to carbon or organic material, sometimes taken from other cases (like water on mineral substrates applied to condensation of hydrocarbons on photochemical aerosols) when not simply ignored. In this work, we used the results of an experiment dedicated to characterize the adsorption isotherm prior to nucleation and the nucleation/condensation saturation threshold of methane and ethane on tholins, an analogous of Titan aerosols.

1. Principle of the work

We used the experimental results of Curtis et al., (2008). For this experiment, the size distribution of the tholin grains and the total volume is fully characterized. Then, the experiment consists in increasing the saturation level from $S=0$ to the critical saturation S_c of methane or ethane beyond which nucleation and condensation starts. The results that we are going to use are the adsorption isotherms of methane (at 45 K) and ethane (75 K) prior to nucleation and the saturation threshold that trigger nucleation.

We used the Langmuir isotherm to reproduce methane adsorption and the Brunauer-Emmett-Teller (BET) isotherm for the ethane adsorption. The choice of the isotherm model is primarily defined by the type of the adsorption isotherm, following the IUPAC (Thommes et al., 2005) classification. For each isotherm, the main free parameter is the desorption energy ΔF_{des} of the

adsorbing molecules on the solid substrate. We also have to define other parameters like for instance the molecule jump frequency or the density of adsorption, which are better constrained.

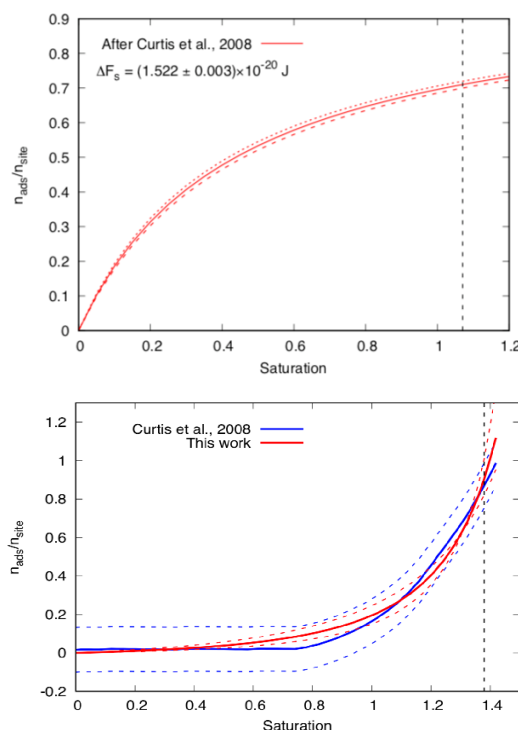


Figure 1: Langmuir isotherm (IUPAC type I) and BET isotherm (IUPAC type III) fitting the methane (top) and ethane (bottom) adsorption as a function of the saturation ratio

Once the desorption isotherm is understood and the corresponding parameters are defined for each molecules, we can study the condensation threshold. We used a microphysical model based on the classical equations of nucleation (Pruppacher and Klett, 1997). However, we used the relevant adsorption isotherm to calculate the nucleation rate, instead of the simpler rule used in the classical laws. We simulate as closely as possible the Curtis et al.,

(2008). We reproduce, with a time resolved model, the increase of the saturation and we compute at each time step the nucleation rate and condensation growing rate. Our model predicts the size of the condensation droplets which appear, then we can also compute the opacity of the methane layer that forms due to condensation and we are able to define an optical threshold for the transmission.

We use this model over the complete range of possible values for m (that is between -1 and +1) and for each values of m , we simulate the nucleation and the adsorption up to trigger the condensation. This allows to define, for each gas, the range of value for m which is consistent with the observed critical saturation.

2. Main results

We find that methane adsorption follows very well the Langmuir adsorption isotherm, as already noted by Curtis et al. (2008). We find that the desorption energy is $\Delta F_{\text{des}} = 1.5220 \pm 0.0715 \times 10^{-20} \text{ J}$ if we include all the uncertainties and the wetting factor $m = 0.994 \pm 0.001$. Ethane adsorption, fitted with a BET isotherm, only allows to retrieve $\Delta F_{\text{sub}} - \Delta F_{\text{des}} = 2.723 \times 10^{-21} \text{ J}$ where ΔF_{sub} is the ethane latent heat of sublimation. The interpretation of the ethane adsorption will be discussed because it is not straightforward, and it could be understood in at least two different ways. However, the value of m can be retrieved regardless the way to interpret the isotherm, and we find the value $m = 0.966 \pm 0.007$.

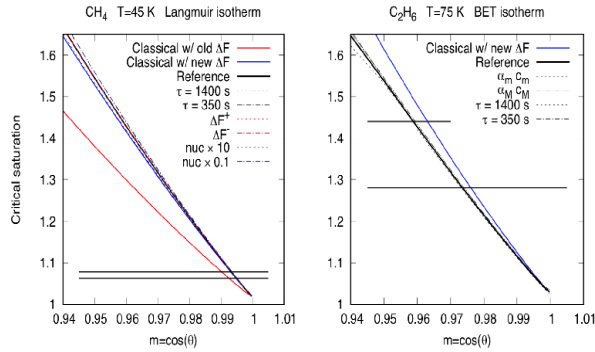


Figure 2: Critical threshold as a function of m for different parameters of the microphysical model for methane (left) and ethane (right). The horizontal layers indicate the experimental values of the actual critical observed in Curtis et al., 2008 experiment.

3. Consequences on microphysical models

The last part of this work will consist in investigating the consequences of our finding on microphysical models. First we show how and why the nucleation laws should be modified to account for a more detailed description of the adsorption isotherm. We also investigate the consequences on the actual case of Titan (and possibly on other planets with photochemical aerosols). We find that because m is close to 1, finally, the fine detail of the adsorption or nucleation have little impact provided that the desorption energy is well known. For cases with smaller values of m , (< 0.97) the type of isotherm used to calculate nucleation may matter.

We finally give suggestion of what could be done to go further. Indeed, we used experimental results done with one specific type of tholins, while we know that the composition of laboratory tholins varies with their formation condition. Their chemical composition can also evolve with time while they get older. This could have an impact on the physical parameters that govern adsorption and nucleation. Of course, such study should also be performed with other gases relevant to planetary atmospheres.

4. References

- Curtis, D. B., Hatch, C. D., Hasenkopf, C. A., Toon, O. B., Tolbert, M. A., McKay, C. P., and Khare, B. N. (2008). Laboratory studies of methane and ethane adsorption and nucleation onto organic particles: Application to Titan's clouds. *Icarus*, 195:792–801.
- Pruppacher, H. R. and Klett, J. D. (1997). *Microphysics of Clouds and Precipitation* (2nd edition). Kluwer Academic Publishers, Dordrecht : The Netherlands.
- Thommes, M., Kaneko, K., Neimark, A. V., Olivier, P., Rodriguez-Reinoson, F., Rouquerol, J., and Sing, K. S. W. (2015). "Physisorption of gases, with special reference to the evaluation of surface area and pore size distribution (IUPAC Technical Report)". *Pure and Applied Chemistry*, De Gruyter, 87:9–10.

Identifying the enigmatic Haystack and HASP ice clouds observed by CIRS in Titan's stratosphere

Delphine Nna-Mvondo (1, 2), Carrie M. Anderson (1), Robert E. Samuelson (1, 3)

(1) NASA GSFC, Greenbelt, MD, USA, (2) Universities Space Research Association (USRA), Columbia, MD, USA,
(3) University of Maryland, College Park, MD, USA (delphine.nnamvondo@nasa.gov / Fax: +1-301-6146522)

Abstract

Stratospheric ice clouds have been repeatedly observed in Titan's atmosphere by the Cassini Composite InfraRed Spectrometer (CIRS) since the Cassini spacecraft entered into orbit around Saturn fourteen years ago. However, their chemical composition is still undetermined. For some of them, co-condensation could be a formation mechanism. We present the laboratory experiments we have conducted and the results we have obtained with the aim to identify particularly two perplexing observed stratospheric clouds, the Haystack and the High-Altitude South Polar (HASP) ice clouds.

1. Introduction

In addition to the tropospheric convective methane clouds, a second type of cloud system is observed in Titan's stratosphere. Ices clouds of crystalline cyanoacetylene (HC_3N , ν_6 band at 506 cm^{-1}) and dicyanoacetylene (C_4N_2 , ν_8 band at 478 cm^{-1}) are detected in CIRS far-infrared (far-IR) spectra, at high latitudes during the northern winter [1] [2]. CIRS far-IR data also show that during mid to late northern winter on Titan, thin nitrile ice clouds extend globally from 85°N to at least 55°S . These ices exhibit several overlapping broad-emission features due to low-energy lattice vibrations [3] (Table 1). Recently, a massive stratospheric ice cloud system, called the High-Altitude South Polar (HASP) cloud, has been discovered in Titan's early southern winter stratosphere at high southern latitudes [4]. Most of Titan's stratospheric ice clouds form as a result of vapor condensation processes, composed of pure organic cyanides (like HC_3N and C_4N_2) but also of mixed nitriles and hydrocarbons. The first co-condensed nitrile ice feature dominated by a mixture of HCN and HC_3N ices, has been identified in the CIRS limb spectra, peaking at 160 cm^{-1} [3]. Most of

Titan's organic vapors condense to form successive ice shells on Titan's aerosol particles as the vapors cool while descending throughout Titan's stratosphere. However, depending on the vapor abundances, local atmospheric temperatures and saturation vapor pressures, these gases enter altitude regions in Titan's stratosphere where they can simultaneously saturate, and co-condense. During co-condensation, the ice particles mixed together and are no longer isolated into successive shells of pure ices (layered ice). The presence of other CIRS-observed stratospheric ices, such as the unidentified Haystack peaking at $\sim 220\text{ cm}^{-1}$ and the HASP peaking near 200 cm^{-1} are puzzling since not any pure condensed vapor matches their emission features. In the present work, we have investigated if co-condensed mixed ices could contribute to the Haystack and HASP emission features.

Table 1: Spectral assignment of the stratospheric ice clouds detected by CIRS.

Stratospheric ices detected by CIRS	Far-IR emission features (cm^{-1})
HC_3N	$506 (\nu_6)$ crystalline
C_4N_2	$478 (\nu_8)$ crystalline
Nitrile composite ice	160 (peak)
Haystack	220 (peak)
HASP	200 (peak)

2. Experimental methodology

We have performed experiments using the SPECTroscopy of Titan-Related ice AnaLogs (SPECTRAL) high-vacuum chamber set up at NASA Goddard Space Flight Center. The SPECTRAL chamber (Fig. 1) has been designed specifically for measuring laboratory transmission spectra of thin ice films of pure and mixed ices, at Titan-appropriate temperatures ($70 - 130\text{ K}$) from the near to far-infrared region, i.e. from 11700 cm^{-1} to 50 cm^{-1} . The vapors were deposited at low temperatures from 30 K to 160

K, and the resulting ice thicknesses were determined, the ice phase were analysed by FTIR spectroscopy and their optical constants computed.

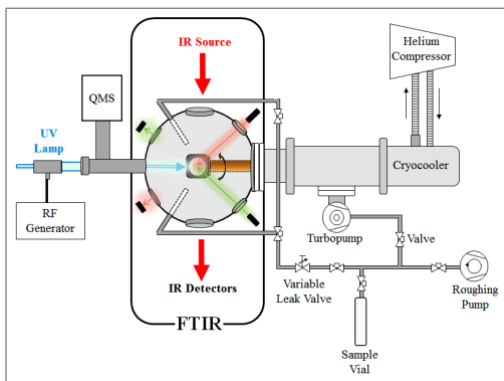


Figure 1: Schematic of the SPECTRAL high-vacuum chamber experimental setup at NASA GSFC.

3. Results

3.1 Results: HASP study

We have co-condensed vapor mixtures of HCN- HC_3N , C_6H_6 - HC_3N and C_6H_6 -HCN at 110 K and analysed the resulting mixed ices (Fig. 2). HCN, HC_3N , C_6H_6 are gases co-condensing at the pressures, temperatures and altitude where the HASP cloud is observed.

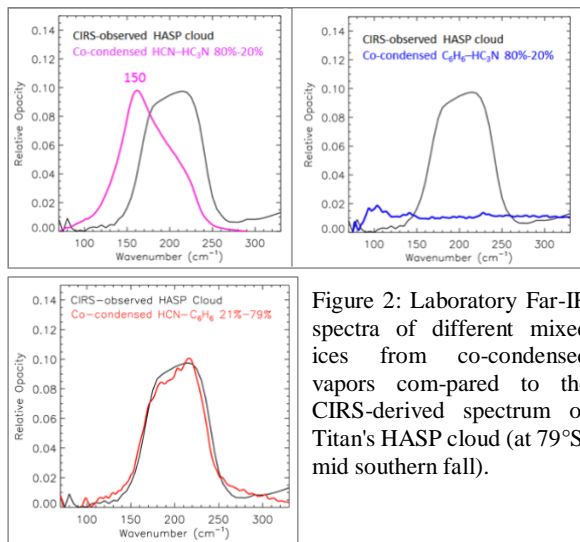


Figure 2: Laboratory Far-IR spectra of different mixed ices from co-condensed vapors compared to the CIRS-derived spectrum of Titan's HASP cloud (at 79°S, mid southern fall).

The spectrum of co-condensed thin ice film from mixed vapors of 20% HCN- 80% C_6H_6 deposited at 110 K is a good match for the HASP emission feature at 200 cm^{-1} . This result demonstrates that the chemical composition of the HASP cloud is consistent with a mixed C_6H_6 -HCN ice, formed via co-condensation.

3.2 Results: Haystack study

Spectra of crystalline HCN ice and crystalline propionitrile ($\text{C}_2\text{H}_5\text{CN}$) ice obtained from pure vapors deposited at 110 K and 135 K, respectively were obtained (Fig. 3). They do not match the Haystack emission feature at 220 cm^{-1} .

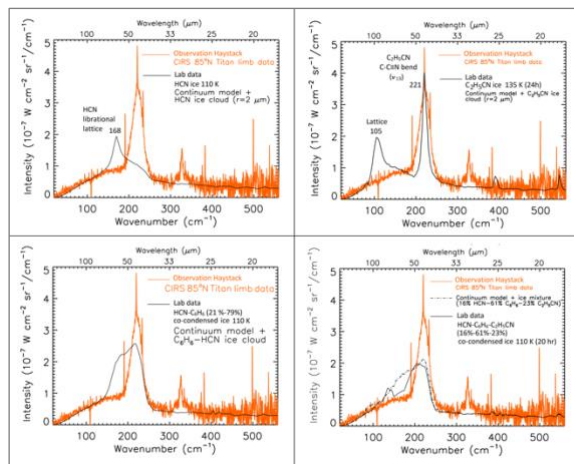


Figure 3: Laboratory Far-IR spectra of different mixed ices from co-condensed vapors compared to the CIRS-derived spectrum of Titan's Haystack cloud (at 85°N).

Comparing our laboratory spectra of different mixed ices containing HCN, C_6H_6 , $\text{C}_2\text{H}_5\text{CN}$ to the CIRS data (Fig. 3), we do not find any good match for the Haystack emission feature yet, but further experiments with other co-condensed ices are currently in progress.

Acknowledgements

D.N.-M acknowledges research funding support by the NASA Postdoctoral Program at NASA GSFC, administered by the USRA. C.M.A. and R.E.S. acknowledge funding from both the Cassini Project and the CDAP.

References

- [1] Anderson, C.M., Samuelson, R.E., Bjoraker, G.L., Achterberg, R.K.: Particle size and abundance of HC_3N ice in Titan's lower stratosphere at high northern latitudes. *Icarus*, Vol. 207, pp. 914-922, 2010.
- [2] Anderson C.M., Samuelson, R.E., Achterberg, R.K., Barnes, J.W., Flasar, F.M.: Subsidence-induced methane clouds in Titan's winter polar stratosphere and upper troposphere. *Icarus*, Vol. 243, pp. 129-138, 2014.
- [3] Anderson C.M., Samuelson, R.E.: Titan's aerosol and stratospheric ice opacities between 18 and $500\text{ }\mu\text{m}$: Vertical and spectral characteristics from Cassini CIRS. *Icarus*, Vol. 212, pp. 762-778, 2011.
- [4] Anderson, C.M., Nna-Mvondo, D., Samuelson, R.E., Achterberg, R.K., Flasar, F.M., Jennings, D.E., Raulin, F.: Titan's High Altitude South Polar (HASP) Stratospheric Ice Cloud as observed by Cassini CIRS. In: AAS/DPS Meeting Abstracts, Vol. 49, p 304.10, 2017.

Photodesorption and Photochemistry of Titan's Aerosol Analogs

Benjamin Fleury(1), **Murthy S. Gudipati** (1), Isabelle Couturier-Tamburelli (2), Nathalie Carrasco(3)
(1) Science Division, Jet Propulsion Laboratory, California Institute of Technology, 4800 Oak Grove Drive, Pasadena, California 91109, USA; (2) Aix-Marseille Université, CNRS, PIIM, UMR 7345, 13013 Marseille, France ; (3) Université Versailles St-Quentin, Sorbonne Universités, UPMC Univ. Paris 06, CNRS/INSU, LATMOS-IPSL, 11 Blvd. d'Alembert, 78280 Guyancourt, France. (gudipati@jpl.nasa.gov)

Abstract

Titan's lower stratosphere and troposphere (lower atmosphere) receives UV-depleted longer wavelength photons. These photons are not energetic enough to cause photochemical transformations of molecules in the gas phase. However, aerosols with longer wavelength absorption could transfer that energy to other molecules resulting indirect photo-induced transformations.

1. Introduction

While Titan's upper atmosphere is photochemically very active, due to the aerosols and clouds it is often assumed that Titan's lower atmosphere is photochemically inert. However, our recent works has clearly shown that even at wavelengths that pass through the upper atmosphere unattenuated (longer than 300 nm) into the lower atmosphere, photochemistry continues to happen (Couturier-Tamburelli et al. 2014; Couturier-Tamburelli, Pietri, & Gudipati 2015; Couturier-Tamburelli et al. 2018; Gudipati et al. 2013). Acetylene, the third most abundant organic molecule in Titan's atmosphere and most abundant unsaturated hydrocarbon, cannot be photoexcited at >300 nm wavelengths, either in the gas-phase or in condensed-phase such as clouds or ice. Our goal is to understand what would happen if acetylene condenses on larger aerosols that could absorb photons reaching the lower atmosphere. Would acetylene become reactive? Indeed, our results indicate it does.

2. Results

We irradiated pure acetylene ice deposited on sapphire window at 50 K using highly de-focused (to avoid multiphoton processes) laser at 355 nm. We did not find any significant change in the infrared and

ultraviolet absorption spectra of acetylene. Subsequently, we deposited ~20 nm thick acetylene ice film on a ~600 nm thick Titan's aerosol analog coated sapphire window (produced through discharge). When irradiated at 355 nm, we found significant depletion of acetylene based on infrared spectra. We have repeated similar studies at longer wavelengths, whereby the depletion effect was not as dramatic.

During these studies we have also monitored gas-phase molecular abundancies using quadrupole mass spectrometry. After careful experimentation and data analysis, we recognized that two processes work in parallel when acetylene coated Titan's aerosol analogs are bombarded with >300 nm photons: (a) photodesorption of acetylene, which accounts to about 25% of the total acetylene loss. Remaining 75% acetylene should have been chemically bonded with the aerosol.

Acknowledgements

This work was carried out at the Jet Propulsion Laboratory, California Institute of Technology, was under a contract with the National Aeronautics and Space Administration (NASA). Funds were provided through NASA Solar System Workings Program.

References

- Couturier-Tamburelli, I., Gudipati, M. S., Lignell, A., Jacovi, R., & Pietri, N. 2014, *Icar*, 234, 81
- Couturier-Tamburelli, I., Pietri, N., & Gudipati, M. S. 2015, *Astronomy & Astrophysics*, 578, A111
- Couturier-Tamburelli, I., Pietri, N., Le Letty, V., Chiavassa, T., & Gudipati, M. 2018, *ApJ*, 852, 117
- Gudipati, M. S., Jacovi, R., Couturier-Tamburelli, I., Lignell, A., & Allen, M. 2013, *Nature Communications*, 4, 1648

Spatial and temporal variability of Titan's detached haze layer during the Cassini mission

Benoît Seignovert (1,2), Pascal Rannou (2) Robert A. West (1)
 (1) JPL, California Institute of Technology, Pasadena, California, USA, (2) GSMA, UMR CNRS 6089, Université Reims
 Champagne-Ardenne, France (research@seignovert.fr)

Abstract

The 13 years of the Cassini mission provide a unique dataset monitoring the evolution of Titan's atmosphere during almost half a Titan year. We present here a systematic survey of the vertical extinction profiles retrieved between 300 to 700 km with an atmospheric limb multiple scattering model. We sampled the ISS NAC CL1-UV3 dataset on the entire Cassini mission, from 2004 (during the northern winter) to the end of the mission in 2017 (after the summer solstice). The spatial and temporal variations observed bring new perspectives on the cycle of the detached haze layer and its interaction with the dynamics.

1. Introduction

Titan is the only moon of the solar system with a thick hazy atmosphere. Above its main haze, the presence of a small *detached* haze layer was first observed by Voyagers [1] during the 80's flyby of Titan. The analysis of this strange feature by Rages & Pollack confirms the existence of an excess of extinction located around 350 km, associated with a peak of particles density and a local depletion 50 km below [2]. Its horizontal extent was very stable in altitude and reported at all the southern latitudes up to 45°N where it connects to the northern polar hood.

In 2004, 25 years later, Cassini ISS cameras reveal a similar haze layer located at 500 km [3]. Its altitude remains stable up to 2007 [4] when it starts to collapse down to 380 km in 2010 and disappeared in 2012 after the equinox [5]. As predicted by 2-3D Global Circulation Models (GCMs) [6, 7, 8], the detached haze layer reappeared in 2016 [9] at 480 km but reveals a more complex behavior than expected.

Therefore, a detailed analysis of the spatial variability of Titan's detached haze layer is required to fully understand these seasonal variations.

2. Data & Method

Our survey is conducted on 137 images taken by the Cassini Image Sub-System Narrow Angle Camera (ISS/NAC) with the ultra-violet (CL1-UV3) filters (Fig. 1) to get the highest temporal and phase coverage. The average time between two pictures is 40 Earth days (2.5 Titan days). Due to orbital constraints, no data were recorded between 03/08-01/09 and 10/10-09/11 but at least 90 % of our sample are separated by less than 120 Earth days (7.5 Titan days).

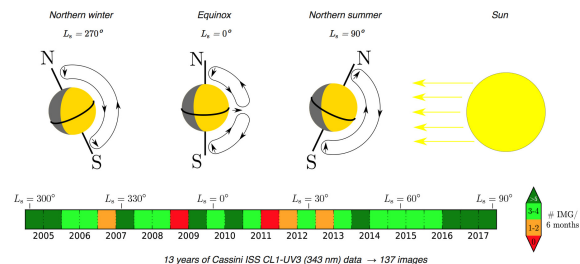


Figure 1: Seasonal evolution of Titan's illumination and global scale circulation during the Cassini mission (2004-2017) with a color-coded time series of the ISS/NAC CL1-UV3 images used in this study.

The dataset is calibrated using CISSCAL and the signal to noise ratio on the limb profile is improved by deconvolving the images with a Poisson maximum a posteriori method (PMAP) using the point spread function (PSF) calculated in-flight [10]. The navigation of the images is initialized with the Spice routines and the location of the center of Titan is refined by searching the best alignment on the limb.

To retrieve haze extinction coefficient profiles from the I/F profiles, we calculated single-scatter I/F in a spherical-shell geometry between 300 and 700 km altitude [2, 11]. The multiple scattering is taken into account with a correction factor based on a plane-parallel radiative transfer model using atmosphere properties fitted on nadir observations (see [9] for more details).

3. Results

Between 2004 and 2007, the detached haze layer appears as a continuous layer at 500 km from the south pole to the north pole where its thickness increases before its junction with the polar hood at 60°N (Fig. 2).

Around the equinox in 2009, the depletion below the detached layer starts to drop down to 350 km. We notice that this drop appears quicker in the southern hemisphere. The merge with the main haze occurs in 2012 around 300 km with a similar pattern as predicted by GCMs but with a temporal offset of 30° in solar longitude.

Between 2012 and 2015, no consistent detached haze is reported even if some sporadic local depletions could be observed. It's only in early 2016 that the detached haze reappears as a continuous layer from the northern hemisphere down to the south pole where it connects with the main haze.

Finally, in 2017 after the northern summer solstice, the detached haze layer splits into two layers at 520 km in the southern hemisphere and at 470 km in the northern hemisphere. This feature reveals a complex unanticipated underlying dynamics. This pattern could be an early stage before the formation of a new persistent detached haze layer during the northern summer.

Additionally, when it was possible, we conducted a small-scale analysis to estimate the longitude and the dusk/dawn variability (not presented here). Our first results show second order variations which reveal short timescales events (alternation day/night, wave activity, ...).

Overall, the observations match the large scale behavior predicted by the GCMs however we report a temporal offset during the collapse and the reappearance of the detached haze layer. We also show that the detached haze layer is not always a constant layer but varies with latitude, revealing a complex dynamics which should provide valuable constraints for future GCMs.

References

- [1] Smith et al. (1981). Encounter with Saturn: Voyager 1 Imaging Science Results. *Science* 212, 163–191. doi:10.1126/science.212.4491.163
- [2] Rages & Pollack (1983). Vertical distribution of scattering hazes in Titan's upper atmosphere. *Icarus*, 55, 50–62. doi:10.1016/0019-1035(83)90049-0
- [3] Porco et al. (2005). Imaging of Titan from the Cassini spacecraft. *Nature* 434, 159–168. doi:10.1038/nature03436

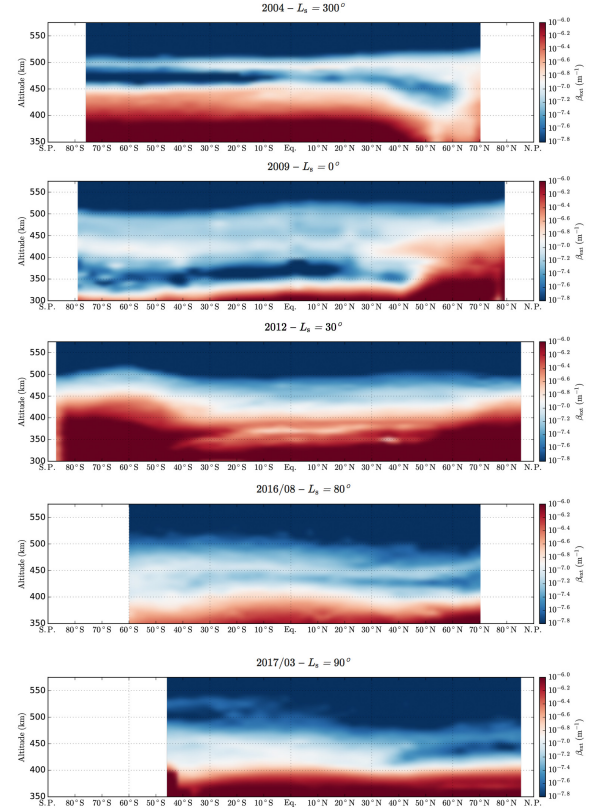


Figure 2: Latitudinal variability of the extinction profiles of the detached layer during the northern winter (top), the equinox (middle) and the northern summer solstice (bottom).

- [4] Seignovert et al. (2017). Aerosols optical properties in Titan's detached haze layer before the equinox. *Icarus* 292, 13–21. doi:10.1016/j.icarus.2017.03.026
- [5] West et al. (2011). The evolution of Titan's detached haze layer near equinox in 2009. *Geophysical Research Letters*, 38(6), 2–5. doi:10.1029/2011GL046843
- [6] Rannou et al. (2002). A wind origin for Titan's haze structure. *Nature* 418, 853–856. doi:10.1038/nature00961
- [7] Lebonnois et al. (2012). Titan global climate model: A new 3-dimensional version of the IPSL Titan GCM. *Icarus* 218, 707–722. doi:10.1016/j.icarus.2011.11.032
- [8] Larson et al. (2015). Microphysical modeling of Titan's detached haze layer in a 3D GCM. *Icarus* 254, 122–134. doi:10.1016/j.icarus.2015.03.010
- [9] West et al. (2018). The seasonal cycle of Titan's detached haze. *Nature Astronomy*. doi:10.1038/s41550-018-0434-z
- [10] West et al. (2010). In-flight calibration of the Cassini imaging science sub-system cameras. *Planet. Sp. Sci.* 58, 1475–1488. doi:10.1016/j.pss.2010.07.006
- [11] Rannou et al. (1997). A new interpretation of scattered light measurements at Titan's limb. *J. Geophys. Res. Planets* 102, 10997–11013. doi:10.1029/97JE00719

Titan's polarization phase curves with Cassini/ISS

N. Ilic (1), A. García Muñoz (1), B. Seignovert (2), R.A. West (3), B. Knowles (4), P. Lavvas (2)

- (1) Technische Universität Berlin, Berlin, Germany
- (2) Université de Reims Champagne-Ardenne, Reims, France
- (3) Jet Propulsion Laboratory, Pasadena, USA
- (4) CICLOPS/Space Science Institute, Boulder, USA

Abstract

The sunlight reflected by Titan's atmosphere is strongly polarized at phases near quadrature. This Rayleigh-like behavior has provided key clues towards the understanding of the aggregate nature of Titan's ubiquitous haze [1, 2]. We are compiling the polarization phase curves of Titan with data collected with Cassini's Imaging Science Subsystem (ISS). The ISS dataset covers the spectrum from the UV to the NIR, and phase angles from nearly zero degrees (full illumination) to 150 degrees, thereby extending the observations made by the Voyager and Pioneer spacecraft decades ago. The ISS dataset confirms the older trends in Titan's polarization, i.e. high fractional polarizations at quadrature that increase towards the shorter wavelengths. The ISS dataset also shows new insight thanks to the relatively good phase sampling and to the availability of data at wavelengths affected by methane absorption. Since we have spectrally-resolved phase curves in both brightness and polarization, we are investigating the optimal way to combine that information towards the optimal characterization of Titan's atmosphere.

1. Introduction

Ref. [3] discusses Titan's brightness phase curves obtained from images taken with ISS's Narrow Angle Camera (NAC) and non-polarizing filters. We are currently extending that analysis to include images taken with the Wide Angle Camera (WAC) as well as with polarizing filters. Figure 1 shows a brightness phase curve obtained with four instrument configurations on the CB2 filter. The configurations are: *i*) NAC without polarizing filters (*Photometric Data (NAC)* in the Legend); *ii*) NAC with 3 polarizing filters offset by 60 deg (*Polarimetric Data (NAC)*); *iii*) WAC without polarizing filters (*Photometric Data (WAC)*); *iv*) WAC with two polarizing filters at right angles (*Polarimetric Data (WAC)*).

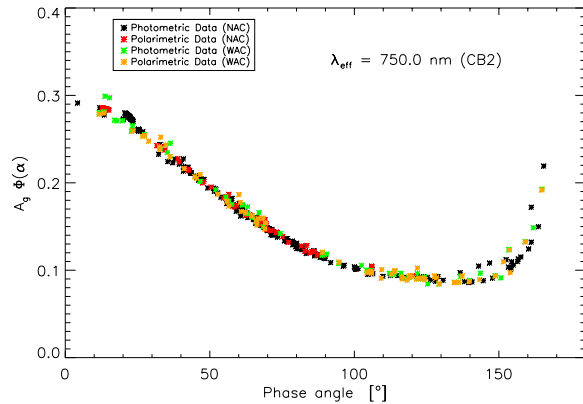


Figure 1. Cassini/ISS brightness phase curve of Titan taken with the CB2 filter (effective wavelength of ~750 nm). The four datasets correspond to measurements done with: NAC without polarizers; NAC with 3 polarizing filters; WAC without polarizers; WAC with 2 polarizing filters.

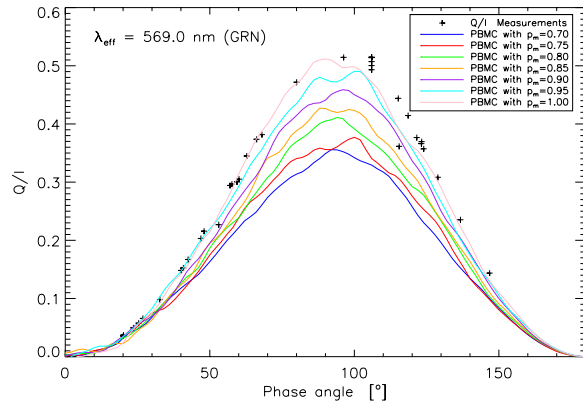


Figure 2. Titan's fractional polarization measured with the NAC and the green filter (effective wavelength of ~570 nm). NAC measurements result in the two elements of the Stokes vector for linear polarization, Q and U , referred to the camera axes. To produce the phase curve in the graph, we have rotated the reference plane for each datapoint so that the rotated Stokes elements $U=0$ and $Q>0$. The solid curves are models calculated with a Monte Carlo algorithm that solves the multiple scattering problem in Titan's atmosphere [4]. The models assume that the normalized elements of the scattering matrix $F_{ij}/F_{11}(\theta)$ are Rayleigh-like, meaning that $F_{ij}/F_{11}(\theta)|_{\text{aerosol}} \propto F_{ij}/F_{11}(\theta)|_{\text{Rayleigh}}$. p_m parameterizes the maximum single-scattering polarization in $F_{12}/F_{11}(\theta)|_{\text{aerosol}}$, which occurs for $\theta=90$ deg. The model simulations suggest that values of $p_m \sim 1$ are required to reproduce the observations. The wiggles in the synthetic phase curves are due to poor statistics in the Monte Carlo simulations, which for these exploratory examples are run with 10^5 photons.

Figure 2 shows the fractional polarization Q/I obtained with the NAC and the green filter (effective wavelength of ~ 570 nm). The fractional polarization is obtained from the ratio of Q and I . Figure 3 shows the corresponding curve for Q .

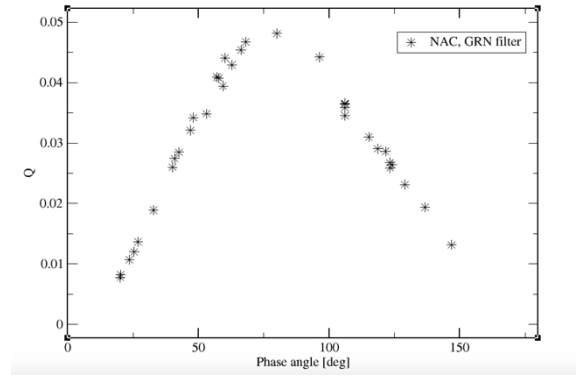


Figure 3. Phase curve for Q , obtained with the NAC and the green filter.

Figures 2-3 show that the sampling in phase angle is quite complete, and allows to trace the polarization behavior up to phase angles of 150 deg. At this wavelength, Titan reaches a maximum fractional polarization of 50 percent. This value is representative of the haze optical properties over the entire atmosphere and within less than one optical depth from the atmospheric top. Figure 4 compiles some images of Titan's disk and shows the orientation of the emergent electric field.

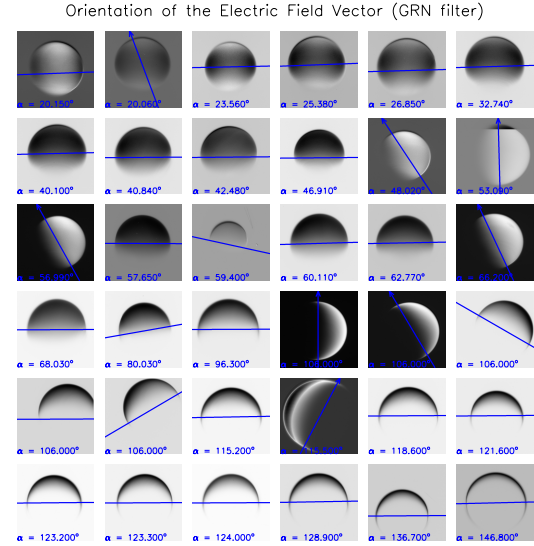
We are currently addressing the interpretation of the polarization curves with a Monte Carlo model that solves the multiple scattering problem in the atmosphere [5]. For the time being, we have assumed that the scattering matrix of the aerosols can be described in the form $F_{ij}/F_{11}(\theta)|_{\text{aerosol}} \propto F_{ij}/F_{11}(\theta)|_{\text{Rayleigh}}$. In particular, for $F_{12}/F_{11}(\theta)|_{\text{aerosol}} = p_m F_{12}/F_{11}(\theta)|_{\text{Rayleigh}}$, where p_m is a user-defined parameter that represents the maximum polarization for single scattering.

The comparison of models to observations should result in valuable constraints on the aerosol sizes near the top of the atmosphere. Our initial exploration suggests that the haze layer to which the measurements are sensitive is strongly polarizing, with nearly full polarization in single scattering ($p_m \sim 1$, Fig. 2). Our analysis complements the linear polarization investigation of Titan's atmosphere during the DISR descent [6], which is probably relevant to lower altitudes than those probed by the phase curves here.

Summary and future work

The Cassini/ISS polarization phase curves that we are preparing represent a valuable dataset for the characterization of Titan's aerosols. This emphasizes the diagnostics possibilities offered by polarimetry, which complements other remote sensing techniques. The next steps include the interpretation of the phase curves with multiple scattering models.

Figure 4. Orientation of the electric field in images taken with the NAC and the green filter. In these images, it is possible to infer all three I , Q and U elements of the Stokes vector.



References

- [1] Tomasko, M.G. & Smith, P.H. Photometry and polarimetry of titan: Pioneer 11 observations and their implications for aerosol properties. *Icarus*, 51, 65-95, 1982.
- [2] West, R.A. et al., Voyager 2 photopolarimeter observations of Titan. *JGR*, 88, 8699-8708, 1983.
- [3] García Muñoz, A., Lavvas, P. & West, R.A. Titan brighter at twilight tan in daylight. *Nature Astronomy*, 1, Article number: 0114, 2017.
- [4] West, R.A., Knowles, B., et al. In-flight calibration of the Cassini imaging science sub-system cameras. *PSS*, 58, 1475-1488, 2010.
- [5] García Muñoz, A. & Mills, F.P. Pre-conditioned backward Monte Carlo solutions to radiative transport in planetary atmospheres. *Fundamentals: Sampling of propagation directions in polarizing media*. *A&A*, 573, id.A72, 2015.
- [6] Tomasko, M.G. et al., Limits on the size of aerosols from measurements of linear polarization in Titan's atmosphere. *Icarus*, 204, 271-283, 2009.

A Vapor Pressure Database for Modeling Planetary Atmospheres

Erika Barth

Southwest Research Institute, Boulder, Colorado, USA (ebarth@boulder.swri.edu)

Abstract

Atmospheric modeling involving the condensation process, such as in photochemical or microphysical models, requires knowledge of the vapor pressure of the condensing species as a function of temperature. Additionally latent heat values, which can be related to the vapor pressure through the Clausius-Clapeyron equation, are important when modeling energy transport processes. Online reference sites such as the NIST Chemistry WebBook contain formulations of the vapor pressure for many species found in the planetary atmospheres of our solar system. However the NIST equations most often report data for the liquid phase, whereas at the colder temperatures in outer solar system, these species would condense as ices. There have been some works in the literature that compile lists of vapor pressure equations and data points for sublimation, but an online database allowing the user to perform calculations or create plots over a desired temperature range is lacking.

1. Introduction

Understanding the validity of vapor pressure and latent heat equations for a given temperature range is of great importance to a variety of researchers across the planetary science community. Applications include photochemical modeling, microphysical modeling, energy balance models, general circulation models, planetesimal formation models, and interpreting spacecraft observations.

Ices are prevalent in the outer solar system and have been detected at the surface of many planetary bodies. The prevalence of methane (CH_4) in outer planet atmospheres leads to an abundance of hydrocarbons created through photochemistry. The molecular nitrogen composition, particularly on Titan and Pluto, also results in creation of a number of nitrile species. Thus, modeling the condensation process in the outer solar system requires knowledge of vapor pressure and latent heat values as a function of temperature, often

well below the triple point of the various (hydrocarbon and nitrile) species present in these planetary atmospheres.

The National Institute of Standards and Technology (NIST) Chemistry WebBook (Linstrom and Mallard: <http://webbook.nist.gov/chemistry/>) provides the most complete online database of vapor pressure, latent heat, and triple point temperature/pressure values. [4] is an example, containing temperature relations for the vapor pressures of nine hydrocarbons anticipated to condense in Neptune's atmosphere. [1] has been widely cited by the modeling community. They give both liquid and ice forms of the vapor pressure equations for a dozen species, including the alpha and beta phases of some ices (e.g., N_2 , CO). [2] more recently conducted an extensive study of sublimation vapor pressure lab data in order to evaluate the measurements for low temperatures and construct a polynomial fit (similar in form to Brown and Ziegler's equation)

While the works cited above have proved extremely useful, they do have their limitations, particularly with reference to the outer planet atmospheres in our solar system – the NIST database primarily due to a lack of data for low temperatures and Fray and Schmitt due to gaps in the number of species where suitable equations could be derived and (as with [1]) the computational expense of their equation. What would be most useful for the research community would be the ability to graphically compare all reference equations for a given species across any desired temperature range. Such a task is currently being undertaken by developing the software tools described below.

2. Vapor Pressure Modules

A number of Fortran 90 modules will be written so that these equations can be called directly from existing code. Each reference equation is coded into a separate function, named with the condensing species and the specific reference name (e.g. nist, author's name). The complete citation and temperature range

(if available) cited from the original source is listed. A wrapper function (e.g., `vapor_press_CH4`) is then used to access the specific reference equation for a given species, providing an input argument of phase and reference ID. There is a similar looking `latent_heat_CH4` wrapper function with calls to the collected latent heat equations.

Each condensing species is self-contained in its own 'database' module. All module names take the same form, `database_formula`, where formula is the molecular formula of the condensing species, e.g. `CH4`, `C2H6`, `C2H2`, etc. Within each module, the vapor pressure and latent heat functions all follow the same naming convention as well, for ease of use.

The Fortran modules will be designed such that they can be compiled/run on their own or called from an existing model. Fortran was chosen as many of the models listed in Sec. 1 have this language as their heritage, and also a Fortran compiler is typically available on the systems of most researchers. Additionally, Fortran code can be called from C, Python, and IDL. The modules will be tested on both Linux and Windows platforms and have currently been compiled using both `gfortran` and `ifort` with no problems.

Additionally, a similar set of functions will be coded in Python. These functions also take temperature as an input argument, as well as a string for pressure units for the output value. A reference string is given, similarly to the Fortran functions. If the string is simply 'ref' the function will print a list of available references and their temperature range instead of calculating the vapor pressure or latent heat. The Python dictionary tool allows for the creation of a simple plotting program, where all relevant equations can be accessed simply by giving the species' chemical formula. The vapor pressure module uses only the Python `numpy` package; the `pylab` package is used in the plotting module. Python was chosen as it is freely available and is becoming increasingly used within the research community - both by modelers and non-modelers to visualize their data.

3. Summary

Instructions for compiling and running the Fortran and Python modules will also be provided in the submission to NASA's GitHub. In addition to a separate instructions file, the Python module also contains a help function. The vapor pressure and latent heat calculation functions for all species are contained in a single file (module) for the Python code. There will also be separate python programs for generating the vapor

pressure comparison curves and latent heat curves over a user-supplied range of temperatures. The Fortran code will be a set of separate files (modules) for each species along with a global module file to supply relevant constants (e.g. universal gas constant and unit conversions). To further provide for a wide variety of uses, numerical tables of vapor pressure and latent heat values over a range of temperatures will be generated for all species and submitted to NASA's GitHub.

Initial work on equations relevant to icy species in the Outer Planet atmospheres will be presented here. Future work will include species relevant to exoplanet atmospheres.

Acknowledgements

This work is funded by the NASA PDART program.

References

- [1] Brown, G.N. and W.T. Ziegler: Vapor pressure and heats of vaporization and sublimation of liquids and solids of interest in cryogenics below 1-atm pressure, *Adv. Cryogen. Eng.* Vol. 75, pp. 662-670, 1980. Author, A., Author, B., and Author, C.: First example of a cited article title, *First Example Journal*, Vol. 1, pp. 1-100, 1999.
- [2] Fray, N. and B. Schmitt: Sublimation of ices of astrophysical interest: A bibliographic review, *Planet. Space Sci.*, Vol. 57, pp. 2053-2080, 2009.
- [3] P.J. Linstrom and W.G. Mallard, Eds., *NIST Chemistry WebBook*, NIST Standard Reference Database Number 69, National Institute of Standards and Technology, Gaithersburg MD, 20899, <http://webbook.nist.gov>.
- [4] Moses, J. I., M. Allen, and Y. L. Yung. Hydrocarbon nucleation and aerosol formation in Neptune's atmosphere. *Icarus* 99, 318-346, 1992.